ANTICANCER RESEARCH *38*: 4267-4272 (2018)
doi:10.21873/anticanres.12723

Visualizing Energy Charge in Breast Carcinoma Tissues by MALDI Mass-spectrometry Imaging Profiles of Low-molecular-weight Metabolites

NOBUHIRO TORATA[1], MAKOTO KUBO[1], DAISUKE MIURA[2], KENOKI OHUCHIDA[1], YUSUKE MIZUUCHI[1], YOSHINORI FUJIMURA[2], EISUKE HAYAKAWA[2], MASAYA KAI[1], YOSHINAO ODA[3], KAZUHIRO MIZUMOTO[1], MAKOTO HASHIZUME[4] and MASAFUMI NAKAMURA[1]

[1]*Department of Surgery and Oncology, Graduate School of Medical Sciences, Kyushu University, Fukuoka, Japan;*
[2]*Innovation Center for Medical Redox Navigation, Kyushu University, Fukuoka, Japan;*
[3]*Department of Anatomic Pathology, Graduate School of Medical Sciences, Kyushu University, Fukuoka, Japan;*
[4]*Advanced Medicine Innovation Center, Kyushu University, Fukuoka, Japan*

Abstract. *Background/Aim: Metabolomics is widely used for biomarker discovery, but conventional mass-spectrometry extraction procedures lose the spatial localization of metabolites. In this study, we directly analyzed breast carcinoma tissues embedded in frozen tissue microarrays (fTMAs) using MALDI mass-spectrometry imaging (MALDI-MSI). Materials and Methods: A total of 119 breast tissues (84 carcinoma and 35 normal) were used. MSI data were extracted from each tissue. Results: Overall, 185 of 1,915 peaks which were commonly detected in 60% of target areas were subjected to further analysis. One hundred and fifty-two peaks of carcinoma showed significantly higher intensity than normal. Comparing metabolite profiles from carcinoma and normal tissues, energy charge (EC) and the sum of adenosine phosphate compound (AXP) indicated significantly higher intensities in cancerous tissues than normal. But comparisons of EC and AXP among lymph node metastasis, tumor size and tumor subtypes indicated no significant differences. Conclusion: Breast carcinoma tissues had higher EC and AXP values than normal. MALDI-MSI could be a tool for characterizing breast carcinoma.*

Breast cancer continues to be a leading cause of cancer-related deaths among women in the United States (1). Many biological parameters, such as estrogen receptor (ER), progesterone receptor (PR), human epidermal growth factor receptor-2 (HER2) and Ki-67 labeling index are used for subtype classification and deciding therapeutic strategies.

Metabolomics, the comprehensive analysis of metabolites as a compound-level phenotype of genetic alterations, is widely used to elucidate the underlying causes of biological phenomena (2-4), search for disease biomarkers and identification new drug targets. Generally, liquid chromatography mass-spectrometry (MS) or gas chromatography MS are used for metabolomics studies (5-8), however, these methods require extraction processes that results in loss of spatial information regarding the localization of identified metabolites. MS imaging (MSI), which can determine the distribution of multiple metabolites in sectioned tissues by direct ionization and detection at one time without labeling (9-10), has been applied for *in situ* imaging of relatively abundant macromolecules, such as proteins, peptides and lipids (11-15).

In this study, low molecular weight metabolites in breast carcinoma tissues embedded in frozen TMA (16) were visualized and distinct metabolites between carcinoma and normal tissue were identified. Furthermore, their usefulness as cancer biomarkers was assessed.

Materials and Methods

Ethics statement. This study was approved by the Ethics Committee of Kyushu University (approval number: 22-149, 23-64) and conducted according to the Ethical Guidelines for Human Genome/Gene Research enacted by the Japanese Government and the Helsinki Declaration. All patients provided signed informed consent approving the use of their tissues for unspecified research purposes.

Patients, tissues and fTMA construction. Breast carcinoma tissues were obtained from patients who underwent breast resection at our institution, and clinicopathological characteristics of tissue samples

Correspondence to: Makoto Kubo, 3-1-1 Maidashi, Higashi-ku, Fukuoka 812-8582, Japan. Tel: +81 926425441, e-mail: mkubo@tumor.med.kyushu-u.ac.jp

Key Words: Mass spectrometry imaging, breast cancer, frozen tissue, tissue microarray, energy charge, matrix-assisted laser desorption/ionization-time of flight- MSI, MALDI.

are described in Table I. Tumor stage was assessed according to the classification of the Union for International Cancer Control. Carcinoma and normal areas of individual tissues were confirmed by hematoxylin–eosin (HE) staining after MADLI-MSI analysis. Pathological data for all samples, including ER, HER2 and Ki67 labeling index, were acquired from Kyushu University Hospital. Six fTMA blocks were constructed with 119 breast tissues (84 carcinoma and 35 normal) from 99 patients by a previously described method (16). A classification of ER^+ was defined as ≥1% of tumor cells staining positive for it. Specimens were defined as $HER2^+$ when the HER2 IHC staining was scored as 3+ according to the standard criteria (17, 18) or by fluorescence spectroscopy using *in situ* hybridization, which showed HER2 gene amplification. Ki-67 staining was defined according to staining percentage, with the upper cutoff value set at 20%.

MSI. fTMA embedded breast tissues were sectioned at 10-μm with a cryostat, and then thaw-mounted onto ITO-coated glass slides (Sigma-Aldrich, St. Louis, MO, USA). A matrix solution (5 mg/ml 9-AA in 100% methanol) was sprayed in the draft hood with an airbrush at room temperature (22˚C, 50% humidity). In MSI experiments, three types of MS instruments were used: 1) a single reflectron-type MALDI-TOF-MS (AXIMA Confidence, Shimadzu, Kyoto, Japan) for MSI, 2) a quadrupole ion trap (QIT)-type (AXIMA QIT, Shimadzu) and 3) a TOF/TOF-type (AXIMA Performance, Shimadzu) to identify metabolites. These instruments were equipped with a 337 nm N2 laser with a spot size of 50 μm. In the MSI experiment, data were acquired in negative ionization mode with 50 μm spatial resolution (10 laser shots/data point), and the signals between m/z=50 and 1000 were collected. Metabolites were identified or estimated by comparing MS/MS spectra with standard compounds or databases (METLIN, http://metlin.scripps.edu/; MassBank, http://www.massbank.jp/; and Human Metabolome Database, http://www.hmdb.ca/). Acquired MSI data were processed with the freely available software BioMap (Novartis, Basel, Switzerland). MSI data were normalized by the intensity of matrix (m/z=193.03) in each pixel (XIC: *Extracted*-ion current). The signal intensity of each imaging data in the figure was represented as the normalized intensity. Energy charge (EC) index was calculated by the formula: EC=(ATP + 1/2 ADP)/(ATP + ADP + AMP) and visualized by MSIdV software (19).

Statistical analysis. The Wilcoxon and Steel–Dwass tests were applied to assess significant variances in MSI data between carcinoma and normal tissues using the JMP 11 statistical software package (SAS Institute, Cary, NC, USA). Tumor cell component rate was measured with Adobe Photoshop 11 (Adobe Systems, San Jose, CA, USA).

Results

Signal extraction from representative areas and peak signal comparison between normal and carcinoma tissues. MS signals were extracted from representative normal and carcinoma areas of each tissue which were selected by pathologists. A representative HE staining and MALDI-MSI images of fTMA block are shown in Figure 1A and 1B. Extracted signal waves from the red boxes (Figure 1B) which were corresponding with yellow boxes (Figure 1A) are shown in Figure 1C. 185 of 1,915 peaks signals which were detected in over 60% samples are summarized in Figure 1D. 164 (88.6%) peaks were significantly different and 152 (92.7%) of these peaks indicated higher intensity than normal. A representative MSI image is shown in Figure 1E. The cellular components and stroma rate of each target area were measured by digital captured HE stain image and applied to the subjected signals to correct for the effect of the rate, but it indicated minimal changes after correction (Figure 1F).

Table I. *Clinicopathological characteristics of tissue samples.*

Patients No.	99
Gender (F/M)	98/1
Age (mean±SD range)	57.4±9.8
Operation date	Oct. 2011-Nov. 2013
Operation method	
Breast conservative therapy	48
Mastectomy	51
Sample No. (Tumor/Normal)	119 (84/35)
Tumor signature	
Estrogen receptor (Pos/Neg)	63/21
HER2 (Pos/Neg/Unknown)	21/61/2
Ki-67 index (Pos/Neg)	39/45
Tumor size (mean±SD range)	2.4±1.1 cm
Stage	
0	7
I	34
II	36
III	6
IV	1

No: Number; Pos: Positive; Neg: Negative.

Identifying metabolites that correspond to individual peaks that vary between normal and carcinoma tissues. Among the subjected peaks, 18 metabolites including nucleotide derivatives, redox-related metabolites and central pathway components were identified and listed in Table II. Of note, high-energy phosphate-related metabolites such as ATP and ADP showed high fold change. By comparing metabolite profiles from carcinoma and normal tissues, EC, which is related to ATP, ADP and AMP concentrations, and the sum of adenosine phosphate compound intensities (AXP) in carcinoma areas were significantly higher than normal areas (Figure 2A). To evaluate the energy status in each tissue, we calculated an EC value at each point and constructed images using the same procedures as in other MALDI-MSI experiments. Figure 2B shows representative images of the EC, ATP, ADP and AMP; carcinoma tissues showed higher EC intensities than normal tissues.

Comparing tumor subtypes and high-energy phosphate compound distribution. By comparing tumor subtypes and high-energy phosphate compound distributions, a higher EC

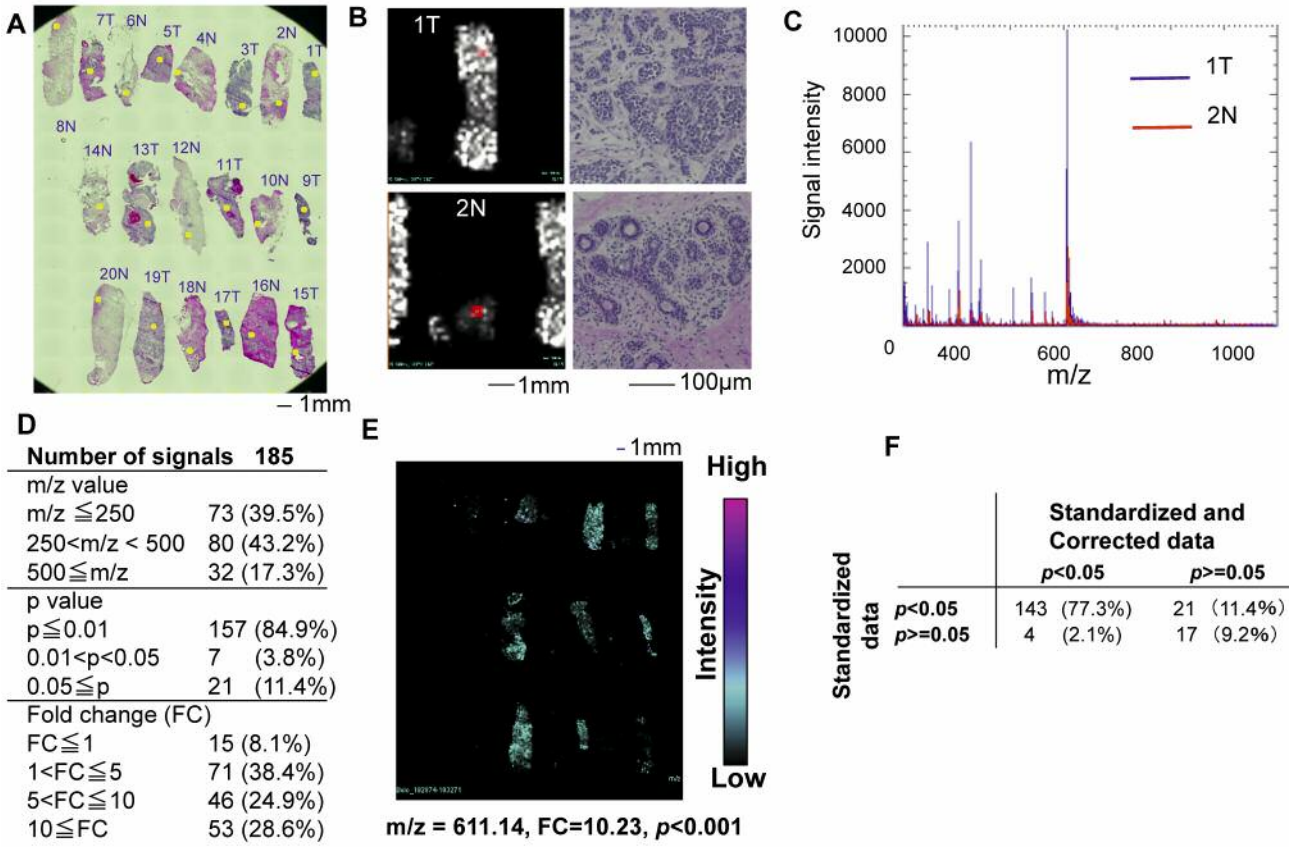

Figure 1. *Signal extraction and comparison between normal and carcinoma tissues. (A) Representative HE-stained images of fTMA blocks. Yellow squares indicate the signal correction area of each sample. (B) MSI and high magnification HE images of representative normal and carcinoma samples, and (C) the corresponding MS signal. (D) Summary of subjected signals. (E) MSI image of representative m/z signals. (F) Comparing significant differences between standardized data and cellular component rate corrected data.*

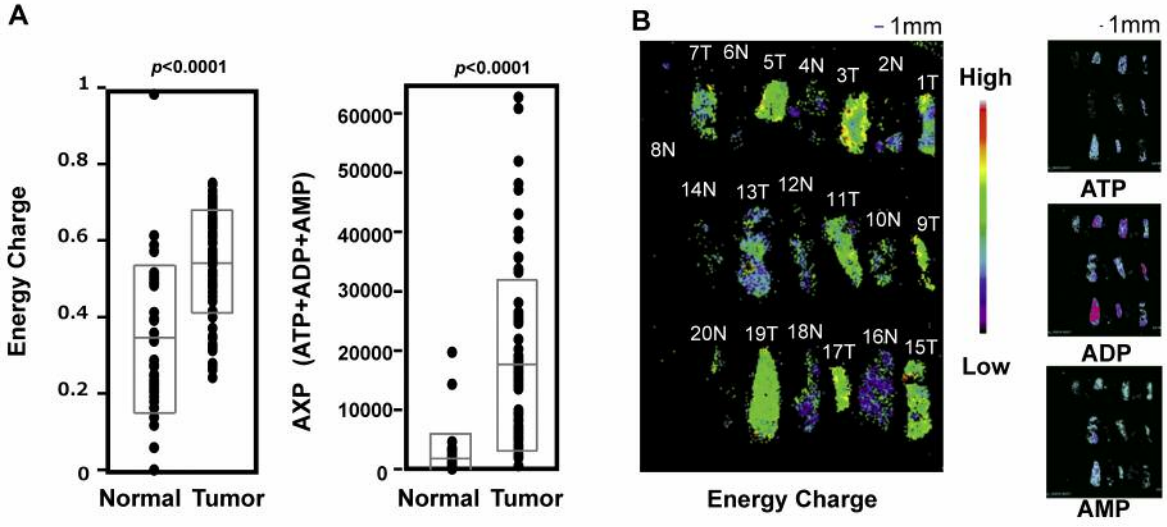

Figure 2. *Identifying metabolites that correspond to subjected peaks and evaluating intensities between tumor and normal tissues. (A) The comparison of the EC index and the sum of adenosine phosphate compound intensities between carcinoma and normal tissues. The box indicates mean value and standard deviation. (B) Calculated EC mapping image with high-energy phosphate compound-related metabolites.*

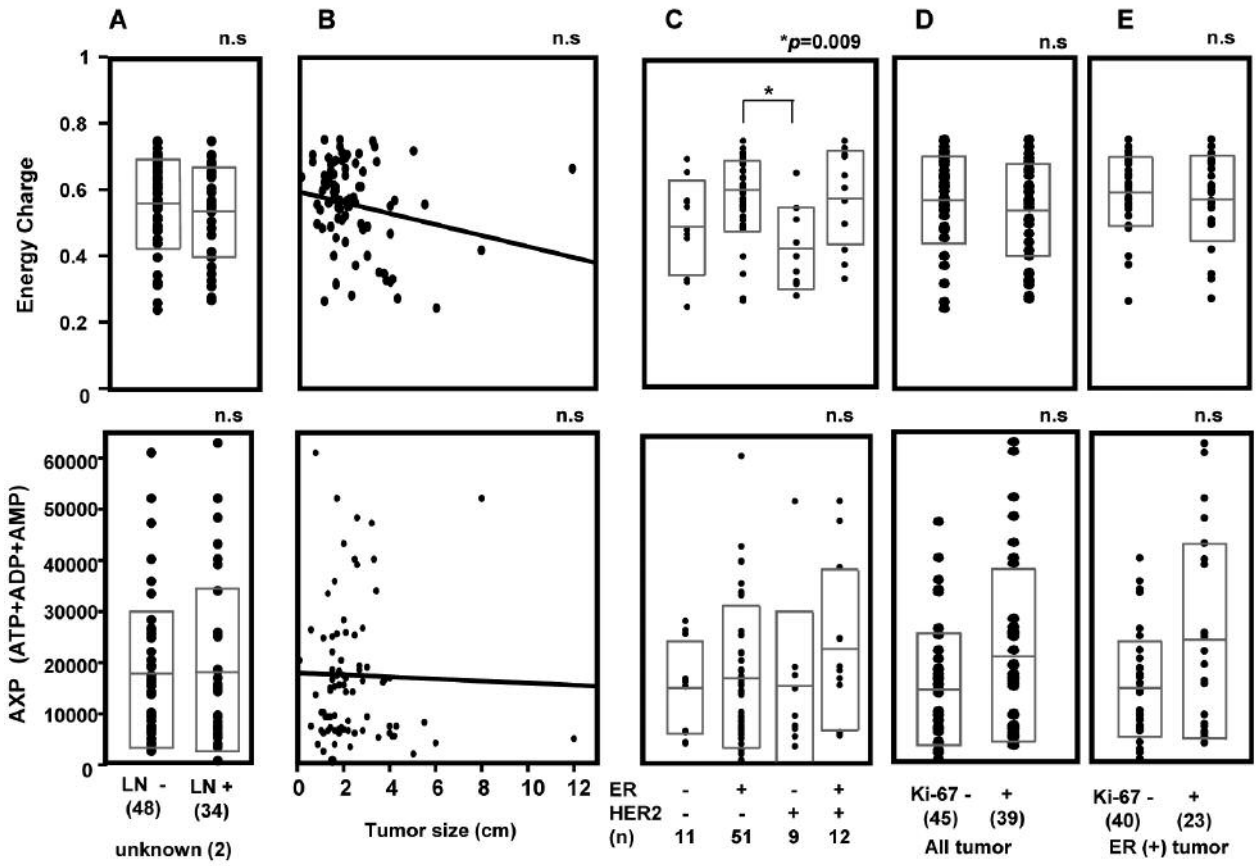

Figure 3. *Comparing tumor signatures and high-energy phosphate compound distributions. EC index (top) and AXP (bottom) comparisons between lymph node metastasis negative and positive tumors (A), Tumor size (B), ER and HER2 status (C), Ki-67 index (all tumors), (D) and Ki-67 index (ER+ tumors) (E). A, B, D, E: Wilcoxon test; C: Steel-Dwass test; LN, Lymph node. The box indicates mean value and standard deviation.*

Table II. *Identified metabolites from 185 subjected signals.*

Metabolite	*m/z*	*T Ave.*	*N Ave.*	*Fold change*	*p*-Value
Adenosine diphosphate (ADP)	426.01	9685.00	1019.93	9.50	0.0001
Adenosine monophosphate (AMP)	346.07	2396.00	696.58	3.44	0.0001
Adenosine triphosphate (ATP)	505.96	5372.56	349.53	15.37	0.0001
ADP-ribose	558.06	165.08	84.66	1.95	0.4049
Aspartate	132.10	1084.63	152.29	7.12	0.0001
Citrate	190.99	1113.44	573.57	1.94	0.0001
Deoxycytidine diphosphate (dCDP)	386.03	1579.16	199.92	7.90	0.0001
Fructose 1,6-bisphosphate	339.00	648.18	60.24	10.76	0.0001
Glutamate	146.04	1617.37	430.69	3.76	0.0001
Glutathione	306.09	1327.05	125.29	10.59	0.0001
Glutathione disulfide (GSSG)	611.14	2099.65	205.22	10.23	0.0001
Guanosine diphosphate (GDP)	442.02	1177.95	219.72	5.36	0.0001
N-acetylaspartate	174.01	1664.64	140.25	11.87	0.0001
Nicotinamide adenine dinucleotide (NADH)	664.14	287.56	46.42	6.19	0.0003
UDP-glucose	565.01	2043.60	509.06	4.01	0.0001
UDP-N-acetylglucosamine (UDP-GlcNAc)	606.04	13956.47	2478.30	5.63	0.0001
Uridine diphosphate (UDP)	402.98	6419.83	724.82	8.86	0.0001
Uridine monophosphate (UMP)	323.03	1161.16	259.97	4.47	0.0001

was observed in $ER^+/HER2^-$ tumors than $ER^-/HER2^+$ tumors, but AXP showed no significant differences among all subtypes (Figure 3C). There were also no significant differences between lymph node metastasis (Figure 3A), tumor size (Figure 3B) or Ki-67 labeling index (Figure 3D and 3E).

Discussion

Characterizing breast carcinoma tissue contributes to tumor classification and decisions about therapeutic strategy. In this study, the distribution of low molecular weight metabolites in breast carcinoma tissues was visualized by a method that combined fTMA and MALDI-MSI and carcinoma tissues were compared with normal tissues. Comparing 185 peaks between carcinoma and normal tissues, 88.6% of the peaks were significantly different and 92.7% of them indicated higher intensities in carcinoma areas than normal areas. This indicated that carcinoma areas included higher low-molecular-weight-metabolites than normal. Eighteen of the 185 peaks were identified as key metabolites and included high-energy phosphate-related compounds such as ATP. The distribution of these peaks was well accorded with carcinoma areas when EC values were visualized in carcinoma versus normal areas. As a result, higher EC and AXP values were found in carcinoma areas than normal areas. This indicated that carcinoma tissues may have remodeled favorable environments for developing their preferred energy status. Similarly, Kubo *et al*. reported that liver metastases from human colon cancer xenografts in mice showed higher EC values than liver parenchyma (20). By comparing tumor subtypes and the distribution of high-energy phosphate compound-related metabolites, $ER^+/HER2^-$ tumors showed higher EC than $ER^-/HER2^+$ tumors. Both ER^- and $HER2^+$ are known risk factors for developing breast cancer (21), but this result suggested that there is a difference between $ER^+/HER2^-$ and $ER^-/HER2^+$ tumors in the status of intracellular energy. Relationships between metabolites and other subtypes including Ki-67 index showed no significant differences. Further investigations on the correlation between EC and subtypes are required. In conclusion, our data showed that breast carcinoma tissues had higher EC and AXP values than normal tissues and that MALDI-MSI could be used as an analytical tool for characterizing breast carcinoma. As Steurer S *et al*. reported, Combining TMA technic and MALDI-MSI is a promising approach for discovering biomarkers and for visualizing the molecular features of carcinoma tissues (22). However, further studies are needed to clarify the molecular mechanisms of EC elevation and identify the signals that were left unidentified in this study.

Acknowledgements

The Authors thank Miyuki Omori, Emiko Manabe and Seiko Sadatomi for their technical assistance. This work was supported by JSPS KANESHI Grant Number 17K10699.

References

1 Siegel RL, Miller KD and Jemal A: Cancer statistics, 2015. CA Cancer J Clin *65(1)*: 5-29, 2015.
2 Griffin JL and Shockcor JP: Metabolic profiles of cancer cells. Nat Rev Cancer *4(7)*: 551-561, 2004.
3 Holmes E, Wilson ID and Nicholson JK: Metabolic phenotyping in health and disease. Cell 134(5): 714-717, 2008.
4 Nicholson JK, Lindon JC and Holmes E: 'Metabonomics': understanding the metabolic responses of living systems to pathophysiological stimuli *via* multivariate statistical analysis of biological NMR spectroscopic data. Xenobiotica *29(11)*: 1181-1189, 1999.
5 Dunn WB and Ellis DI: Metabolomics: Current analytical platforms and methodologies. Trac Trends Anal Chem *24*: 285-294, 2005.
6 Werner E, Croixmarie V, Umbdenstock T, Ezan E, Chaminade P, Tabet JC and Junot C: Mass spectrometry-based metabolomics: Accelerating the characterization of discriminating signals by combining statistical correlations and ultrahigh resolution. Anal Chem *80*: 4918-4932, 2008.
7 Major HJ, Williams R, Wilson AJ and Wilson ID: A metabonomic analysis of plasma from Zucker rat strains using gas chromatography/mass spectrometry and pattern recognition. Rapid Commun Mass Spectrom *20*: 3295-3302, 2006.
8 Pohjanen E, Thysell E, Jonsson P, Eklund C, Silfver A, Carlsson IB, Lundgren K, Moritz T, Svensson MB and Antti H: A multivariate screening strategy for investigating metabolic effects of strenuous physical exercise in human serum. J Proteome Res *6*: 2113-2120, 2007.
9 Caprioli RM, Farmer TB and Gile J: Molecular imaging of biological samples: Localization of peptides and proteins using MALDI-TOF MS. Anal Chem *69*: 4751-4760, 1997.
10 Miura D, Fujimura Y and Wariishi H: In situ metabolomic mass spectrometry imaging: Recent advances and difficulties. J Proteomics *75*: 5052-5060, 2012.
11 Stoeckli M, Chaurand P, Hallahan DE and Caprioli RM: Imaging mass spectrometry: A new technology for the analysis of protein expression in mammalian tissues. Nat Med *7*: 493-496, 2001.
12 Amstalden van Hove ER, Smith DF and Heeren RM: A concise review of mass spectrometry imaging. J Chromatogr A *1217*: 3946-3954, 2010.
13 Vickerman JC: Molecular imaging and depth profiling by mass spectrometry – SIMS, MALDI or DESI? Analyst *136*: 2199-2217, 2011.
14 Miura D, Fujimura Y, Yamato M, Hyodo F, Utsumi H, Tachibana H and Wariishi H: Ultrahighly sensitive *in situ* metabolomic imaging for visualizing spatiotemporal metabolic behaviors. Anal Chem *82*: 9789-9796, 2010.
15 Irie M, Fujimura Y, Yamato M, Miura D and Wariishi H: Integrated MALDI-MS imaging and LC-MS techniques for visualizing spatiotemporal metabolomic dynamics in a rat stroke model. Metabolomics *10(3)*: 473-483, 2014.

16 Torata N, Ohuchida K, Akagawa S, Cui L, Kozono S, Mizumoto K, Aishima S, Oda Y and Tanaka M: Tissue tablet method: an efficient tissue banking procedure applicable to both molecular analysis and frozen tissue microarray. Hum Pathol *45(1)*: 143-152, 2014.

17 Wolff AC, Hammond ME, Schwartz JN, Hagerty KL, Allred DC, Cote RJ, Dowsett M, Fitzgibbons PL, Hanna WM, Langer A, McShane LM, Paik S, Pegram MD, Perez EA, Press MF, Rhodes A, Sturgeon C, Taube SE, Tubbs R, Vance GH, van de Vijver M, Wheeler TM and Hayes DF: American Society of Clinical Oncology/College of American Pathologists guideline recommendations for human epidermal growth factor receptor 2 testing in breast cancer. J Clin Oncol *25(1)*: 118-145, 2007.

18 Wolff AC, Hammond ME, Hicks DG, Dowsett M, McShane LM, Allison KH, Allred DC, Bartlett JM, Bilous M, Fitzgibbons P, Hanna W, Jenkins RB, Mangu PB, Paik S, Perez EA, Press MF, Spears PA, Vance GH, Viale G and Hayes DF: Recommendations for human epidermal growth factor receptor 2 testing in breast cancer: American Society of Clinical Oncology/College of American Pathologists clinical practice guideline update. J Clin Oncol *31(31)*: 3997-4013, 2013.

19 Hayakawa E, Fujimura Y and Miura D: MSIdV: a versatile tool to visualize biological indices from mass spectrometry imaging data. Bioinformatics *32(24)*: 3852-3854, 2016.

20 Kubo A, Ohmura M, Wakui M, Harada T, Kajihara S, Ogawa K, Suemizu H, Nakamura M, Setou M and Suematsu M: Semi-quantitative analyses of metabolic systems of human colon cancer metastatic xenografts in livers of superimmunodeficient NOG mice. Anal Bioanal Chem *400(7)*: 1895-1904, 2011.

21 Pike MC, Spicer DV, Dahmoush L and Press MF: Estrogens, progestins, normal breast cell proliferation, and breast cancer risk. Epidemiol Rev *15*: 17-35, 1993.

22 Steurer S, Seddiqi AS, Singer JM, Bahar AS, Eichelberg C, Rink M, Dahlem R, Huland H, Sauter G, Simon R, Minner S, Burandt E, Stahl PR, Schlomm T, Wurlitzer M and Schluter H: MALDI imaging on tissue microarrays identifies molecular features associated with renal cell cancer phenotype. Anticancer Res *34(5)*: 2255-2261, 2014.

Received April 11, 2018
Revised May 11, 2018
Accepted May 14, 2018